

Methionine Enkephalin Suppresses Osteocyte Apoptosis Induced by Compressive Force through Regulation of Nuclear Translocation of NFATc1

Chisumi Sogi,¹ Nobuo Takeshita,² Wei Jiang,² Siyoung Kim,³ Toshihiro Maeda,² Michiko Yoshida,² Toshihito Oyanagi,² Arata Ito,² Seiji Kimura,² Daisuke Seki,² Ikuko Takano,² Yuichi Sakai,⁴ Ikuma Fujiwara,⁵ Shigeo Kure,¹ and Teruko Takano-Yamamoto^{2,6} 

¹Department of Pediatrics, Graduate School of Medicine, Tohoku University, Sendai, Japan

²Division of Orthodontics and Dentofacial Orthopedics, Graduate School of Dentistry, Tohoku University, Sendai, Japan

³Young Dental Clinic, Ulsan, South Korea

⁴Minamihara Sakai Orthodontic Office, Nagano, Japan

⁵Department of Pediatrics, Sendai City Hospital, Sendai, Japan

⁶Department of Biomaterials and Bioengineering, Faculty of Dental Medicine, Hokkaido University, Sapporo, Japan

ABSTRACT

Mechanical stress stimulates bone remodeling, which occurs through bone formation and resorption, resulting in bone adaptation in response to the mechanical stress. Osteocytes perceive mechanical stress loaded to bones and promote bone remodeling through various cellular processes. Osteocyte apoptosis is considered a cellular process to induce bone resorption during mechanical stress-induced bone remodeling, but the underlying molecular mechanisms are not fully understood. Recent studies have demonstrated that neuropeptides play crucial roles in bone metabolism. The neuropeptide, methionine enkephalin (MENK) regulates apoptosis positively and negatively depending on cell type, but the role of MENK in osteocyte apoptosis, followed by bone resorption, in response to mechanical stress is still unknown. Here, we examined the roles and mechanisms of MENK in osteocyte apoptosis induced by compressive force. We loaded compressive force to mouse parietal bones, resulting in a reduction of MENK expression in osteocytes. A neutralizing connective tissue growth factor (CTGF) antibody inhibited the compressive force-induced reduction of MENK. An increase in osteocyte apoptosis in the compressive force-loaded parietal bones was inhibited by MENK administration. Nuclear translocation of NFATc1 in osteocytes in the parietal bones was enhanced by compressive force. INCA-6, which inhibits NFAT translocation into nuclei, suppressed the increase in osteocyte apoptosis in the compressive force-loaded parietal bones. NFATc1-overexpressing MLO-Y4 cells showed increased expression of apoptosis-related genes. MENK administration reduced the nuclear translocation of NFATc1 in osteocytes in the compressive force-loaded parietal bones. Moreover, MENK suppressed Ca²⁺ influx and calcineurin and calmodulin expression, which are known to induce the nuclear translocation of NFAT in MLO-Y4 cells. In summary, this study shows that osteocytes expressed MENK, whereas the MENK expression was suppressed by compressive force via CTGF signaling. MENK downregulated nuclear translocation of NFATc1 probably by suppressing Ca²⁺ signaling in osteocytes and consequently inhibiting compressive force-induced osteocyte apoptosis, followed by bone resorption. © 2020 The Authors. *JBMR Plus* published by Wiley Periodicals, Inc. on behalf of American Society for Bone and Mineral Research.

KEY WORDS: APOPTOSIS; MECHANICAL STRESS; METHIONIN ENKEPHALIN; NFATc1; OSTEOCYTE

Introduction

Vertebrate skeletons are influenced by various kinds of mechanical stress during daily activities. Mechanical stress stimulates bone remodeling, which occurs through bone formation and resorption, resulting in bone adaptation

to the mechanical stress.⁽¹⁾ Osteocytes are the most abundant cells in bones and are embedded in bone matrices. Osteocytes have their dendritic processes through canaliculi to form an intercellular communication network via gap junctions.^(2,3) Osteocytes perceive mechanical stress as mechanosensors, transform into biochemical signals, and regulate bone

This is an open access article under the terms of the Creative Commons Attribution License, which permits use, distribution and reproduction in any medium, provided the original work is properly cited.

Received in original form October 15, 2019; revised form March 26, 2020; accepted April 21, 2020. Accepted manuscript online April 28, 2020.

Address correspondence to: Teruko Takano-Yamamoto, DDS, PhD, Division of Orthodontics and Dentofacial Orthopedics, Tohoku University Graduate School of Dentistry, 4-1, Seiryomachi, Aoba-ku, Sendai, 980-8575, Japan. E-mail : t-yamamo@m.tohoku.ac.jp

The peer review history for this article is available at <https://publons.com/publon/10.1002/jbm4.10369>.

JBMR® Plus (WOA), Vol. 4, No. 7, July 2020, e10369.

DOI: 10.1002/jbm4.10369

© 2020 The Authors. *JBMR Plus* published by Wiley Periodicals, Inc. on behalf of American Society for Bone and Mineral Research.

remodeling by transmitting signals related to bone formation and resorption.^(4,5)

Osteocytes express receptor activator of nuclear factor kappa B ligand (RANKL), an essential factor for osteoclastogenesis.⁽⁶⁾ Therefore, osteocytes are considered critical for osteoclastogenesis and bone resorption.^(7,8) Importantly, not only living osteocytes, but osteocytes undergoing apoptosis also promote bone resorption.^(9–11) We previously reported that compressive force induces osteocyte apoptosis in the alveolar bones during experimental tooth movement in mice and in cell culture of chick calvaria-derived osteocytes.^(12,13) Our data suggest that osteocyte apoptosis occurs in response to compressive force and induces bone resorption. As to the mechanism of the compressive force-induced osteocyte apoptosis, we revealed that connective tissue growth factor (CTGF) is a molecule that facilitates osteocyte apoptosis.⁽¹³⁾ However, the underlying molecular mechanisms of the compressive force-induced osteocytes apoptosis are not fully understood.

Recent studies have demonstrated that neuropeptides play crucial roles in bone metabolism by regulating osteoblast and osteoclast function.^(14–16) The neuropeptide methionine enkephalin (MENK) is an endogenous opioid encoded by the proenkephalin (PENK) gene. It binds mainly to the delta opioid receptor (DOR) among three opioid receptors: mu, delta, and kappa.⁽¹⁷⁾ It is well known that MENK is expressed in nervous tissue, including the brain and spinal cord. MENK is also expressed in non-nervous tissue, such as bone, heart, pancreas, and kidneys.^(18–21) Its analgesic property is a major function of MENK; moreover, MENK has other functions, including anti-inflammatory effects and regulation of embryonic organ development.^(22,23) On the other hand, long-term administration of opioids to alleviate cancer pain reduces bone mass, suggesting that opioids have a close relationship with bone remodeling.⁽²⁴⁾ MENK is expressed in osteoblasts and mesenchymal stem cells, which are precursors of osteoblasts.^(21,25) In addition, MENK inhibits osteoblast differentiation.⁽²⁶⁾ These findings suggest the inhibitory effect of MENK on bone formation regulating osteoblast differentiation during bone remodeling. However, the role of MENK in bone resorption is still unknown.

McTavish and colleagues reported that PENK enhances apoptosis of human embryonic kidney (HEK) 293 cells and various human tumor cell lines.⁽²⁷⁾ Conversely, activation of DOR suppresses apoptosis of neurons and hepatocytes.^(28,29) These studies suggest that MENK regulates apoptosis positively and negatively depending on cell type. This notion led us to hypothesize that MENK has a novel role in bone resorption by regulating osteocyte apoptosis in response to compressive force. Thus, we first analyzed the expression of MENK in osteocytes and its effect on apoptosis using the mouse model of compressive force loading to cranial bones that we have already established.⁽³⁰⁾ Furthermore, we analyzed the molecular mechanisms of MENK in osteocyte apoptosis induced by compressive force. Nuclear factor of activated T cells (NFAT) induces apoptosis in various types of cells, such as pulmonary artery smooth muscle cells, neurons, and glomerular mesangial cells.^(31–33) Lu and colleagues reported that NFATc2 activation by MENK significantly induces apoptosis of rat C6 glioma cells.⁽³⁴⁾ Therefore, we focused on NFAT to elucidate the MENK-mediated mechanism in osteocyte apoptosis.

Material and Methods

Application of compressive force to mouse parietal bones

Animal experiments were performed in accordance with the regulations for animal experiments and related activities at Tohoku

University. All animal protocols were approved by the Institutional Animal Care and Use Committee of the Tohoku University Environmental and Safety Committee. Mice were housed in groups of up to four animals in a cage and kept at 20°C to 26°C with 12-hour light/dark cycles. They had *ad libitum* access to fresh chow and water.

Six-week-old male Institute of Cancer Research (ICR) mice (Clea Japan, Tokyo, Japan) were anesthetized by i.p. injection of medetomidine (0.3 mg/kg), midazolam (4 mg/kg), and butorphanol (5 mg/kg). A skin incision was made to expose the parietal bones. Two holes were made equidistant from a sagittal suture at the anteroposterior middle of the parietal bones using a round bur attached to a dental drill. The distance between the two holes was 5 mm. A spring that loads 0.2 N of compressive force onto the parietal bones was made by bending a 0.016-inch diameter orthodontic beta-titanium wire (Fig. 1A). The spring was set within the holes in the parietal bones (Fig. 1B), fully covered by skin, and the incision was closed by suturing. In the control group, identical surgical procedures were performed without spring installation.

Either 170 μ L of 1-mg/mL MENK (Sigma-Aldrich, St. Louis, MO, USA), 100 μ L of 25- μ M INCA-6 (Cayman Chemical, Ann Arbor, MI,

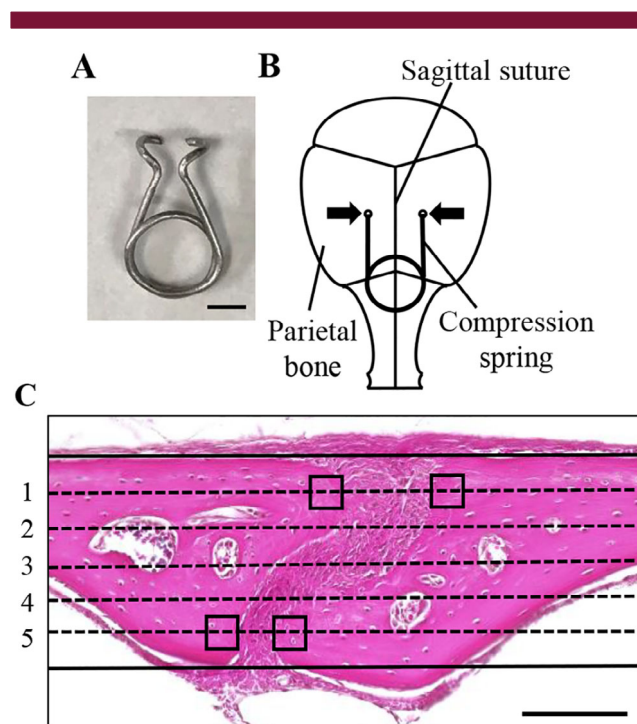


Fig 1 Application of compressive force to mouse parietal bones. (A) A spring for compressive force loading. Scale bar = 2 mm. (B) A schematic diagram of a compression spring placed on mouse parietal bones. To apply 0.2 N of compressive force to the parietal bones, a compression spring was set within holes drilled in the right and left parietal bones of 6-week-old mice. Arrows indicate the direction of compressive force on the parietal bones. (C) For histomorphometric analysis, five lines dividing the thickness of the parietal bones into six equal parts were drawn from dorsal to ventral sides on images of stained sections. The four square fields (30 \times 30 μ m) on the first and fifth lines, in contact with the edges of the right and left parietal bones adjacent to the sagittal suture, were set-up in each specimen as the ROI. Scale bar = 100 μ m.

USA), or 100 μ L of 10- μ g/mL neutralizing antihuman CTGF antibody (PeproTech, Rocky Hill, NJ, USA) were s.c. injected into the parietal bone area. For the negative control, the same volume of PBS or rabbit IgG (Sigma-Aldrich) was injected. A compression spring was installed on parietal bones 2 hours after the MENK and INCA-6 injection, or 6 hours after the CTGF antibody injection. Each injection was given again after surgery. During all of the experiments, mice were carefully monitored and no adverse events were observed.

Histological analysis

After application of the 6-hour compressive force, mice were perfused fixed with 4% paraformaldehyde (PFA; Sigma-Aldrich) under inhalation anesthesia with isoflurane. Calvariae, including the parietal bones, were dissected and immersed in 4% PFA at 4°C overnight. The specimens were decalcified with 20% ethylene-diaminetetraacetic acid (pH 7.4) at 4°C for 7 days. The specimens were then embedded in paraffin, sectioned at 6 μ m, and stained with hematoxylin (Sigma-Aldrich) and eosin (Wako, Osaka, Japan).

Immunohistochemical analysis

Deparaffinized sections were immersed in 0.01 M citrate solution and microwaved for 2 min, then incubated at room temperature (RT) for 30 min. The sections were treated with 10% donkey serum (Sigma-Aldrich) in PBS at RT for 1 hour and incubated with primary antibodies against MENK (1:40; ImmunoStar, New Richmond, WI, USA), DOR (1:100; Abcam, Cambridge, UK), NFATc1 (1:40, Abcam), or NFATc3 (1:50; ProteinTech, Chicago, IL, USA) at RT for 2 hours or at 4°C overnight. In the negative controls, the primary antibodies were replaced by rabbit IgG (Sigma-Aldrich). After washing with 0.3% TritonX-100 (Nacalai Tesque, Kyoto, Japan) in PBS, the sections were incubated with donkey antirabbit-IgG Alexa Fluor 568 (1:500; Invitrogen, Carlsbad, CA, USA) at RT for 1 hour. 4,6-diamidino-2-phenylindole (DAPI; 1:1000; SeraCare, Milford, MA, USA) was used for nuclei detection. Fluorescent signals were visualized using a confocal laser scanning microscope system (C2si; Nikon, Tokyo, Japan). To quantify the fluorescence-positive osteocytes, the fluorescent images were analyzed using ImageJ software (NIH, Bethesda, MD, USA; <https://imagej.nih.gov/ij/>); thresholds of 40 and 255 were used in red channel images. We determined the thresholds by superimposing binary images on the corresponding fluorescent images and confirming overlaps of the signals on the binary images and on the fluorescent images, according to our previous report.⁽³⁵⁾ In our analysis of nuclear translocation of NFAT, fluorescent NFAT signals that contained nuclei of osteocytes were considered positive.

For the detection of active caspase-3, deparaffinized sections were treated with 3% H₂O₂ in methanol and incubated overnight at 4°C with rabbit antihuman cleaved caspase-3 (1:100; Cell Signaling Technology, Danvers, MA, USA) in Can Get Signal Immunos-tain Solution B (Toyobo, Osaka, Japan). After incubation with a peroxidase-conjugated secondary antibody (Histofine Simple Stain Mouse MAX-PO; Nichirei Bioscience, Tokyo, Japan) at RT for 30 min, the signals were visualized with 3,3'-diaminobenzidine tetrahydrochloride (DAB; Nichirei, Tokyo, Japan). The images obtained from caspase-3 immunohistochemistry were analyzed using ImageJ (NIH); thresholds of 0 and 200 were used to quantify the caspase-3-positive osteocytes.

Terminal deoxynucleotidyl transferase-mediated dUTP nick end labeling (TUNEL) staining

Apoptotic cell death was detected using the Apoptosis in situ Detection Kit (Wako Laboratories, Osaka, Japan) according to the manufacturer's protocol. Deparaffinized sections were incubated in prewarmed protease solution at 37°C for 10 min. For labeling 3' terminals of DNA, TdT reaction solution was pipetted onto the sections and incubated at RT for 2 hours. Endogenous peroxidase was inactivated using 3% H₂O₂ for 5 min. Peroxidase-conjugated antibody solution was pipetted onto the sections at 37°C for 10 min. Apoptotic nuclei were then visualized by DAB (Nichirei) at RT for 8 min. Hematoxylin was used for counterstaining. The images obtained from TUNEL staining were analyzed using ImageJ imaging software (NIH). Thresholds of 0 and 160 were used to quantify the TUNEL-positive osteocytes. TUNEL signals overlapping with nuclei of osteocytes were considered positive.

Histomorphometric analysis

Five lines, which divide the thickness of the parietal bones adjacent to the sagittal suture into six equal parts, were drawn from the dorsal to the ventral side on images of stained sections. The four square fields (30 \times 30 μ m) on the first and fifth lines, in contact with edges of the right and left parietal bones adjacent to the sagittal suture, were set-up as the ROI to quantitatively evaluate TUNEL-positive osteocytes, expression of MENK, DOR, and caspase-3 in osteocytes, and nuclear translocation of NFATc1 and NFATc3 in osteocytes (Fig. 1C). The number of osteocytes and the number of TUNEL- or immunohistochemically positive osteocytes in four ROIs in a section were used for calculation of ratio of positive osteocytes.

Cell culture

MLO-Y4 cells were cultured in α modified essential medium (Wako) supplemented with 5% fetal bovine serum (FBS; GE Healthcare, Buckinghamshire, UK), 5% bovine serum (Thermo Fisher Scientific, Waltham, MA, USA), 100-U/mL penicillin, and 100- μ g/mL streptomycin (Thermo Fisher Scientific) on culture plates coated with 0.3-mg/mL type I collagen (Nitta Gelatin, Osaka, Japan). For a MENK administration experiment, cells were seeded onto coated 12-well plates at 1.4×10^4 cells/cm², and MENK was administered after 24 hours. Total mRNA was isolated from cells after 48 hours.

To load compressive force onto MLO-Y4 cells, the cells were seeded at a density of 1.4×10^4 cells/cm² on silicone chambers (size 32 \times 32 mm; Strex, Osaka, Japan) coated with 0.01% poly-D-lysine (Trevigen, Gaithersburg, MD, USA), and 0.3-mg/mL type I collagen and cultured for 2 days. Compressive force was generated by 18% constriction of the chambers using a Strex cell stretch system (Strex); it was loaded onto MLO-Y4 cells for 6 hours. In the control groups, MLO-Y4 cells were cultured on the stretch chambers without compressive force loading. Cells were harvested to isolate total RNA using RNeasy Kit (Qiagen, Venlo, The Netherlands).

Construction of lentiviral vector

The mouse NFATc1 open-reading frame was amplified by PCR and cloned into the XhoI and XbaI sites of the pLV5IN-IRES-ZsGreen1 lentiviral vector (Takara Bio, Shiga, Japan). Viral particles were produced in 293 T Lenti-X cell line (Clontech Laboratories, Palo Alto, CA, USA) using Lentiviral High Titer Packaging Mix

(Takara Bio) following the manufacturer's instructions, and titered using Lenti-X qRT-PCR Titration Kit (Clontech).

RNA isolation from parietal bones

RNA isolation from the mouse parietal bones was performed according to our previous report.⁽³⁶⁾ Mice were sacrificed by cervical dislocation; the parietal bones were quickly dissected. After removing the periosteum and the dura mater, 0.5 mm of parietal bones on either side were isolated and minced with scissors. The specimens were immersed in TRIzol Reagent (Thermo Fisher Scientific) and centrifuged. Total mRNA was then isolated using the RNeasy Kit.

Real-time PCR

cDNA was synthesized from 0.4 µg of total mRNA using a Prime-Script RT Reagent Kit (Takara Bio). Real-time PCR was performed using a Thermal Cycler Dice Real Time System (Takara Bio). The reaction volume was 25 µL, which contained 2 µL of cDNA, 12.5 µL of TB Green Premix Ex Taq II (Takara Bio), and 0.4 µM of sense and antisense primers. The primer sequences are listed in Table 1. The reactions consisted of 40 cycles of 5 s at 95°C and 30 s at 60°C. Relative expression of mRNA was normalized to that of hypoxanthine-guanine phosphoribosyltransferase (HPRT) and analyzed by the $\Delta\Delta CT$ method.

Western blot analysis

Whole-cell proteins from MLO-Y4 cells were prepared using Cell Lytic M Lysis Reagent (Sigma-Aldrich) containing Protease Inhibitor Cocktail (Sigma-Aldrich). The protein samples were boiled in sodium dodecyl sulfate (SDS) sample buffer, separated by SDS polyacrylamide gel electrophoresis, then transferred to polyvinylidene fluoride membranes. The membranes were treated with blocking buffer and incubated overnight at 4°C with rabbit anti-human cleaved caspase-3 (1:500; Cell Signaling Technology) or mouse antihuman glyceraldehyde-3-phosphate dehydrogenase (GAPDH; 1:5000; ProteinTech) antibodies. The membranes were then incubated with horseradish peroxidase-conjugated secondary antibodies, and developed with a chemiluminescence detection reagent. Chemiluminescent signals were acquired using the Fusion FX Imaging System (Vilber Lourmat, Marne La Vallée, France).

Intracellular Ca²⁺ measurement

MLO-Y4 cells were cultured on coated 3.5-cm glass bottom dishes for 24 hours, and MENK was administered into the culture for an additional 24 hours. The cells were loaded with recording buffer (200-mM HEPES, 115-mM NaCl, 5.4-mM KCl, 0.8-mM MgCl₂, 1.8-mM CaCl₂, 13.8-mM glucose, and pH 7.4) containing 5-µM Fura-2 AM (Thermo Fisher Scientific), 1.25-mM probenecid (Thermo Fisher Scientific), and 0.04% Pluronic F-127 (Thermo Fisher Scientific) for 30 min at 37°C. Fluorescent images were captured with an Olympus IX71 (Olympus, Tokyo, Japan) and Hamamatsu EM-CCD digital camera (Hamamatsu Photonics, Shizuoka, Japan) at the rate of 1 frame every 5 s for 5 min. One min after image capturing, 100-nM ionomycin (Wako) was added to the recording buffer. The ratio of fluorescence at wavelengths of 340 and 380 nm were measured in 10 randomly selected cells in each dish, and the average was considered the fluorescence intensity of the sample. The fluorescence intensity in the cells just before ionomycin treatment was regarded as 1. The relative increase in intracellular calcium was assessed using Meta Fluor Software (Molecular Devices, Tokyo, Japan).

Statistical analysis

All data are presented as mean ± SD. Data were statistically analyzed by Student's *t* test to compare differences between two groups. For more than two groups, we used an ANOVA, followed by the Tukey–Kramer test. *p* Values less than 0.05 were considered statistically significant.

Results

Compressive force reduced expression of MENK in osteocytes

Compressive force of 0.2 N loading onto the mouse parietal bones for 6 hours narrowed the suture width between the edges of the right and left parietal bones adjacent to the sagittal suture (Fig. 2A). Histological analysis showed no obvious morphological change of parietal bones and signs of an acute inflammatory response, such as neutrophil infiltration or edema (Fig. 2A). We analyzed expression of MENK and its main receptor DOR in osteocytes by immunofluorescence staining. MENK was expressed in 72.1 ± 3.9% of osteocytes in the nonloaded group, whereas the positive osteocyte ratio was significantly decreased to 34.7 ± 11.5% in the loaded group (Fig. 2B,

Table 1 Primer for Real-Time PCR

Gene name	Forward primer (5'-3')	Reverse primer (3'-5')
PENK	ATGCAGCTACCGCCTGGTTC	CTTGGCTAGCAAGTGGCTCTCA
DOR	CAGACAGCAGACTCCTGAAGCA	ACCGGCTGGGTCAGCTCTAA
NFATc1	TGGAGATGGAAGCAAAGACTG	GCAGACATAGAACTGACTTGGACG
NFATc2	AGGCTTTAGATGGACTGGGTGC	TGATGTCTGGGATGTCTCACAG
NFATc3	GAGTGCCTATAAGTGAGACAC	GGATCCAACTACCTAGAGTAAC
NFATc4	CCCTACCAGACTCATCTCT	TAAGGAGTCTCATAAGCAGG
Caspase-3	CTGCCGGAGTCTGACTGGAA	ATCAGTCCCCTGTCTGTCTCAATG
Caspase-8	CAGGAGGAACAAGGGAAAGCAGTG	GAGAGCACACATCATTAGGGAG
Caspase-9	TCCTGCCTCTTATTCCCAAGTTC	TGTATGCTCTGTGCTCACCTGG
Calmodulin	GTCTGTAACCTCTTGGTGAT	TACCCAGTCTTACAGACTT
Calcineurin A	GTTACGGGTTACTACTGGTT	CTTGAGGCTGTAGTGAATG
Calcineurin B	AACCCTTCAGATGTCTAGTG	GGTAATCAGTACAGGTCAGTC
HPRT	AGGCAGATGGCCACAGGACTA	TTGTTGTTGGATATGCCCTTGACTA

DOR = delta opioid receptor; HPRT = hypoxanthine-guanine phosphoribosyltransferase; PENK = proenkephalin.

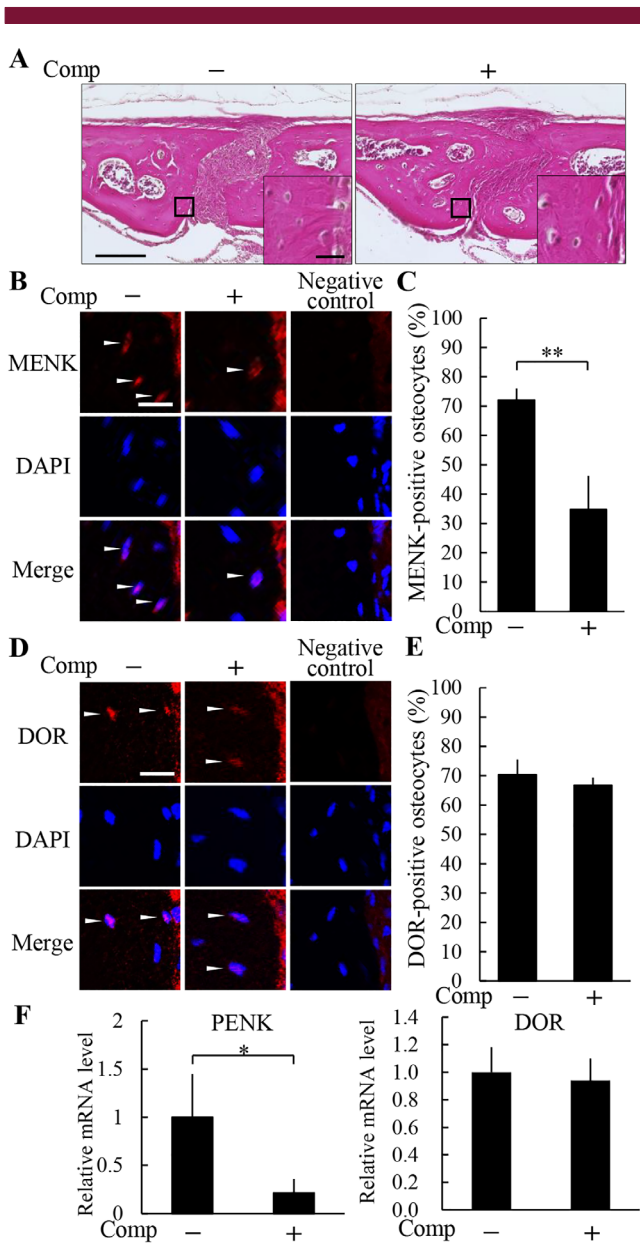


Fig 2 Compressive force reduced expression of methionine enkephalin (MENK) in osteocytes. (A) Histological analysis of the parietal bones at 6 hours after the application of compressive force was performed by H&E staining. A magnified picture of the ROI is shown in the lower right corner of each picture. Scale bar = 100 μ m, and 10 μ m in insets. The expression of MENK (B,C) and the delta opioid receptor (DOR) (D,E) in the parietal bones was analyzed by immunohistochemistry (B,D), and the ratio of positive osteocytes (C,E) was calculated (four animals per group). Arrowheads indicate immunohistochemically positive osteocytes. Scale bar = 10 μ m. Comp = compressive force loading. $**P < 0.01$. (F) Compressive force was loaded onto MLO-Y4 cells for 6 hours and expression of proenkephalin (PENK) and DOR was analyzed by real-time PCR. Comp = Compressive force loading. $*P < 0.05$; $n = 3$.

C). The number of MENK-positive osteocytes and the total number of osteocytes were 7.0 ± 1.7 and 9.8 ± 2.5 , and 3.0 ± 1.4 and 8.5 ± 1.7 in the nonloaded and loaded groups, respectively. In contrast, there was no significant difference in the expression of DOR between the

nonloaded and the loaded groups (Fig. 2D,E). The number of DOR-positive osteocytes and the total number of osteocytes were 7.0 ± 0.8 and 10.0 ± 1.4 , and 7.5 ± 0.6 and 11.3 ± 1.0 in the nonloaded and loaded groups, respectively. The negative controls of MENK and DOR immunohistochemistries showed no apparent immunopositivity in osteocytes (Fig. 2B,D). Consistent with in vivo data, compressive force downregulated expression of PENK mRNA, which encodes MENK, but did not significantly affect DOR mRNA expression in MLO-Y4 cells (Fig. 2F).

A neutralizing CTGF antibody inhibited the decrease in MENK expression in the compressive force-loaded osteocytes

We previously reported that expression of CTGF in osteocytes is upregulated by a compressive force of 0.2 N loading for 6 hours in the same compressive force-loaded mouse model as in the present study.⁽¹³⁾ To examine whether the increased CTGF influences the expression of MENK and DOR in the compressive force-loaded osteocytes, we applied a neutralizing CTGF antibody to the parietal bones prior to compressive force loading. No obvious histological change was observed by administration of the neutralizing CTGF antibody in both the nonloaded and the loaded groups (Fig. 3A). In the nonloaded groups, MENK-positive osteocyte ratios without and with the neutralizing CTGF antibody were $74.1 \pm 8.9\%$ and $69.7 \pm 3.5\%$, respectively; there was no significant difference between these groups (Fig. 3B,C). In the loaded groups, MENK-positive osteocyte ratio without the neutralizing CTGF antibody was $32.2 \pm 7.4\%$; it was significantly lower than the nonloaded groups (Fig. 3B,C). The ratio in the loaded group with the neutralizing CTGF antibody was $71.8 \pm 4.6\%$; it was significantly higher than the loaded group without the neutralizing CTGF antibody and was comparable to the nonloaded groups (Fig. 3B,C). The number of MENK-positive osteocytes and the total number of osteocytes were 8.8 ± 1.5 and 12.0 ± 2.9 , and 7.5 ± 1.0 and 10.8 ± 1.3 in the nonloaded groups without and with the neutralizing CTGF antibody, respectively, and 2.8 ± 1.0 and 8.5 ± 1.7 , and 6.3 ± 1.5 and 8.8 ± 2.4 in the loaded groups without and with the neutralizing CTGF antibody, respectively. DOR-positive osteocyte ratios in the nonloaded groups without and with the neutralizing CTGF antibody were $69.6 \pm 3.9\%$ and $66.8 \pm 5.1\%$, respectively (Fig. 3D,E). The ratios in the loaded groups without and with the neutralizing CTGF antibody were $70.1 \pm 4.8\%$ and $65.4 \pm 6.5\%$, respectively (Fig. 3D,E). There was no significant difference in DOR expression between any of the groups. The number of DOR-positive osteocytes and the total number of osteocytes were 6.8 ± 1.0 and 9.8 ± 1.7 , and 8.0 ± 0.8 and 12.0 ± 1.2 in the nonloaded groups without and with the neutralizing CTGF antibody, respectively, and 8.3 ± 1.3 and 11.8 ± 1.3 , and 7.3 ± 1.0 and 11.3 ± 2.4 in the loaded groups without and with the neutralizing CTGF antibody, respectively.

MENK suppressed osteocyte apoptosis induced by compressive force loading

Our previous study showed that the increased CTGF by compressive force loading induces osteocyte apoptosis in mouse parietal bones.⁽¹³⁾ To evaluate the effect of MENK on the osteocyte apoptosis induced by compressive force, exogenous MENK was s.c. injected into the parietal bone area prior to compressive force loading. There was no obvious histological change caused by MENK administration in the nonloaded and the loaded

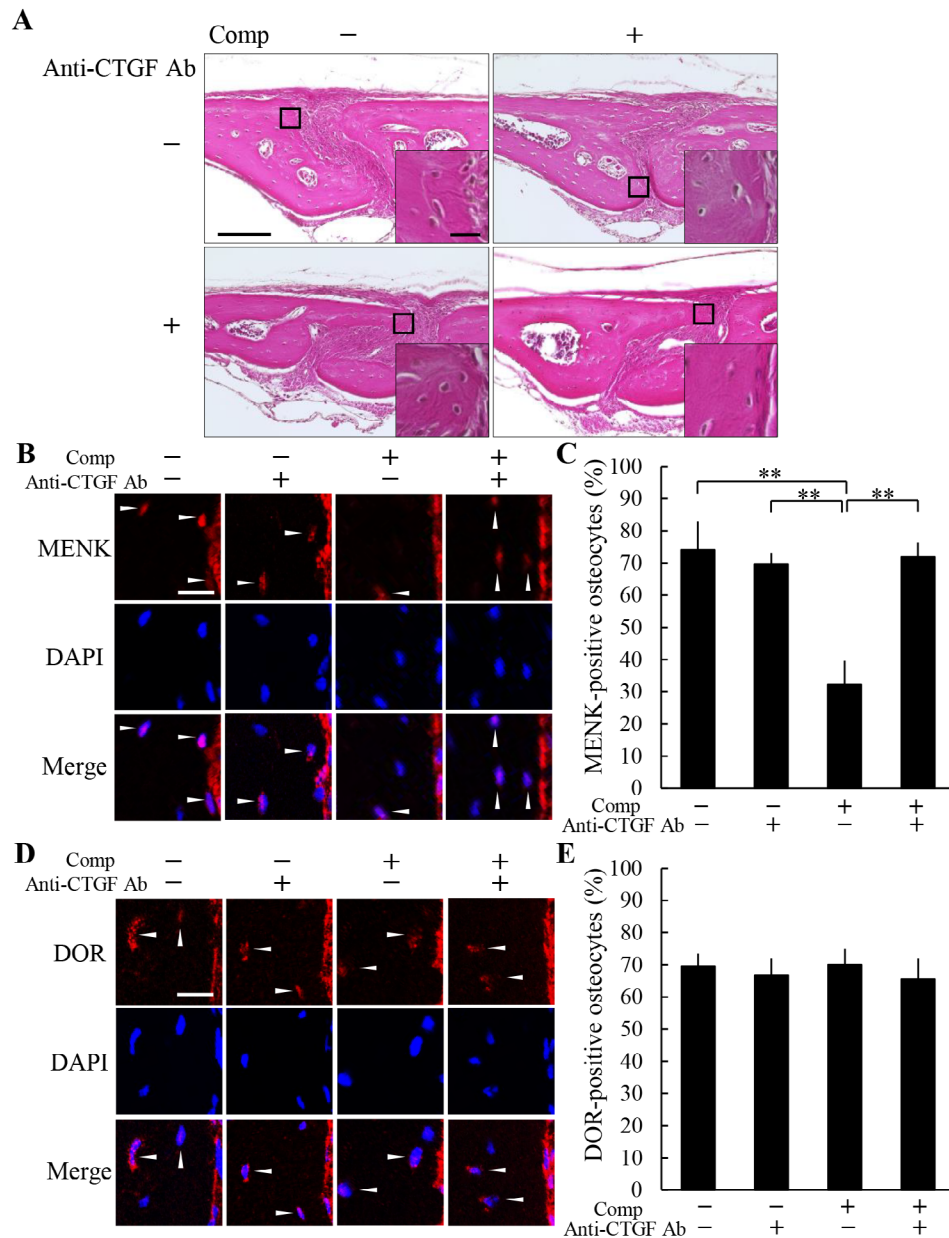


Fig 3 A neutralizing connective tissue growth factor (CTGF) antibody inhibited the decrease in methionine enkephalin (MENK) expression in the compressive force-loaded osteocytes. (A) Histological analysis of the parietal bones at 6 hours after application of compressive force was performed by H&E staining. A neutralizing CTGF antibody was injected s.c. into the parietal bone area prior to the application of compressive force. A magnified picture of the ROI is shown in the lower right corner of each picture. Scale bar = 100 μ m, and 10 μ m in insets. The expression of MENK (B,C) and the delta opioid receptor (DOR) (D,E) in the parietal bones of each group was analyzed by immunohistochemistry (B,D), and the ratio of positive osteocytes (C,E) was calculated (four animals per group). Arrowheads indicate immunohistochemically positive osteocytes. Scale bar = 10 μ m. Comp = compressive force loading, anti-CTGF Ab = neutralizing CTGF antibody. $**P < 0.01$.

groups (Fig. 4A). TUNEL-positive osteocyte ratios without and with MENK in the nonloaded groups were $16.8 \pm 5.1\%$ and $16.4 \pm 4.2\%$, respectively (Fig. 4B,C). In the loaded group without MENK, TUNEL-positive osteocyte ratio significantly increased to $35.2 \pm 6.2\%$ compared with the nonloaded groups (Fig. 4B,C). On the other hand, the MENK administration in the loaded group significantly decreased TUNEL-positive osteocyte ratio to

$17.9 \pm 8.9\%$ compared with the loaded group without MENK, resulting in the comparable TUNEL-positive osteocyte ratio to the nonloaded groups (Fig. 4B,C). The number of TUNEL-positive osteocytes and the total number of osteocytes were 1.5 ± 0.6 and 8.8 ± 1.0 , and 1.5 ± 0.6 and 9.0 ± 2.2 in the nonloaded groups without and with MENK, respectively, and 3.8 ± 0.5 and 10.8 ± 1.0 , and 1.8 ± 1.0 and 9.8 ± 1.9 in the loaded groups

without and with MENK, respectively. We also examined expression of active caspase-3 in osteocytes. In the nonloaded groups, caspase-3-positive osteocyte ratios without and with MENK were $13.3 \pm 3.2\%$ and $10.5 \pm 2.8\%$, respectively (Fig. 4D,E). In the loaded groups, caspase-3-positive osteocyte ratio without MENK was $23.5 \pm 5.6\%$; it was significantly higher than the nonloaded groups (Fig. 4D,E). The ratio in the loaded group with MENK was

$10.9 \pm 3.0\%$; it was significantly lower than the loaded group without MENK and comparable to the nonloaded groups (Fig. 4D,E). The number of caspase-3-positive osteocytes and the total number of osteocytes were 1.5 ± 0.6 and 11.0 ± 1.9 , and 1.3 ± 0.5 and 11.8 ± 2.1 in the nonloaded groups without and with MENK, respectively, and 2.3 ± 0.5 and 9.8 ± 1.7 , and 1.3 ± 0.5 and 11.3 ± 1.3 in the loaded groups without and with

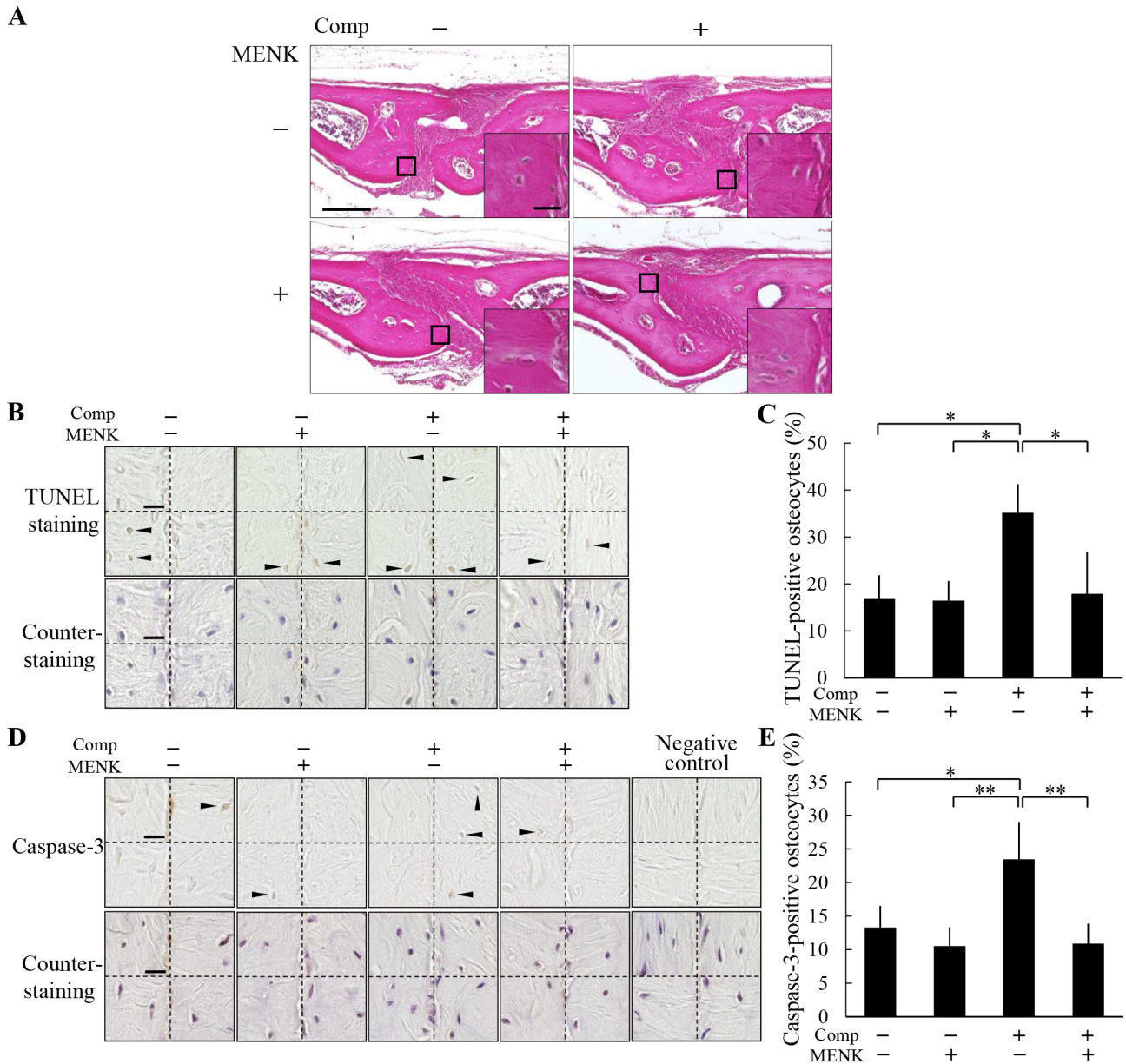


Fig 4 Methionine enkephalin (MENK) suppressed osteocyte apoptosis induced by compression force loading. (A) Histological analysis of the parietal bones at 6 hours after application of compressive force was performed by H&E staining. MENK was injected s.c. into the parietal bone area prior to application of compressive force. A magnified picture of the ROI is shown in the lower right corner of each picture. Scale bar = 100 μ m, and 10 μ m in insets. (B) TUNEL staining and subsequent counterstaining with hematoxylin of the parietal bones were performed. All four ROIs in a section in each group are shown. Arrowheads indicate TUNEL-positive osteocytes. Scale bar = 10 μ m. (C) TUNEL-positive ratio of osteocytes was calculated (four animals per group). (D) Caspase-3 immunohistochemistry and subsequent counterstaining with hematoxylin of the parietal bones were performed. All four ROIs in a section in each group are shown. Arrowheads indicate caspase-3-positive osteocytes. Scale bar = 10 μ m. (E) Caspase-3-positive ratio of osteocytes was calculated (four animals per group). Comp = compressive force loading. * $P < 0.05$, ** $P < 0.01$.

MENK, respectively. The negative control of caspase-3 immunohistochemistry showed no apparent immunopositivity in osteocytes (Fig. 4D).

Compressive force induced nuclear translocation of NFATc1 in osteocytes

We next examined expression of NFATs in the mouse parietal bones and MLO-Y4 cells. Fig. 5A shows NFATc1 and NFATc3 mRNAs were highly expressed in these tissues and cells, whereas expression levels of NFATc2 and NFATc4 mRNAs were quite low. We further analyzed nuclear translocation of NFATc1 and NFATc3 of osteocytes in the compressive force-loaded parietal bones. The ratio of NFATc1-positive nuclei was $30.0 \pm 6.0\%$ in the nonloaded group, whereas the ratio was significantly increased to $65.2 \pm 8.0\%$ in the loaded group (Fig. 5B,C). The number of NFATc1-positive nuclei and the total number of nuclei were 3.3 ± 0.5 and 11.0 ± 1.6 , and 6.0 ± 0.8 and 9.3 ± 1.3 in the nonloaded and loaded groups, respectively. In contrast, there was no significant difference in the ratio of NFATc3-positive nuclei between the nonloaded and the loaded groups (Fig. 5D, E). The number of NFATc3-positive nuclei and the total number of nuclei were 3.0 ± 0.8 and 10.5 ± 1.3 , and 2.8 ± 1.0 and 10.3 ± 1.5 in the nonloaded and loaded groups, respectively. The negative controls of NFATc1 and NFATc3 immunohistochemistries showed no apparent immunopositivity in osteocytes (Fig. 5B,D).

The induction of osteocyte apoptosis by compressive force loading is dependent on NFATc1

To examine whether the nuclear translocation of NFATc1 induced by compressive force loading stimulates osteocyte apoptosis;

INCA-6, an inhibitor of nuclear translocation of NFATs, was applied to the parietal bones prior to compressive force loading. No obvious histological changes were observed after INCA-6 administration in the nonloaded and the loaded groups (Fig. 6A). In the compressive force-loaded group, TUNEL-positive osteocyte ratio was $37.0 \pm 3.5\%$ without INCA-6 administration, whereas INCA-6 significantly decreased the ratio to $18.0 \pm 5.7\%$ (Fig. 6B,C). The number of TUNEL-positive osteocytes and the total number of osteocytes were 3.8 ± 1.3 and 10.0 ± 2.7 , and 1.5 ± 0.6 and 8.3 ± 1.3 without and with INCA-6 administration, respectively. Under the compressive force-loaded condition, caspase-3-positive osteocyte ratio was $22.9 \pm 5.8\%$ without INCA-6 administration, whereas INCA-6 significantly decreased the ratio to $9.2 \pm 1.1\%$ (Fig. 6D,E). The number of caspase-3-positive osteocytes and the total number of osteocytes were 2.3 ± 0.5 and 10.0 ± 1.6 , and 1.0 ± 0 and 11.0 ± 1.4 without and with INCA-6 administration, respectively. To determine a direct effect of NFATc1 on osteocyte apoptosis, we examined expression of apoptosis-related genes in NFATc1-overexpressing MLO-Y4 cells (Fig. 6F). Expression levels of caspase-3, caspase-8, and caspase-9 mRNAs in MLO-Y4 cells were significantly increased by overexpression of NFATc1 (Fig. 6G). Moreover, overexpression of NFATc1 upregulated cleaved caspase-3 protein expression in MLO-Y4 cells (Fig. 6H).

MENK inhibited nuclear translocation of NFATc1 in the compressive force-loaded osteocytes

Next, we examined whether MENK regulates nuclear translocation of NFATc1 and NFATc3. In the nonloaded groups, ratios of NFATc1-positive nuclei without and with MENK were $26.7 \pm 4.9\%$ and $30.6 \pm 6.6\%$, respectively (Fig. 7A,B). In the loaded group without MENK, the ratio of NFATc1-positive nuclei was $65.6 \pm 7.4\%$, a

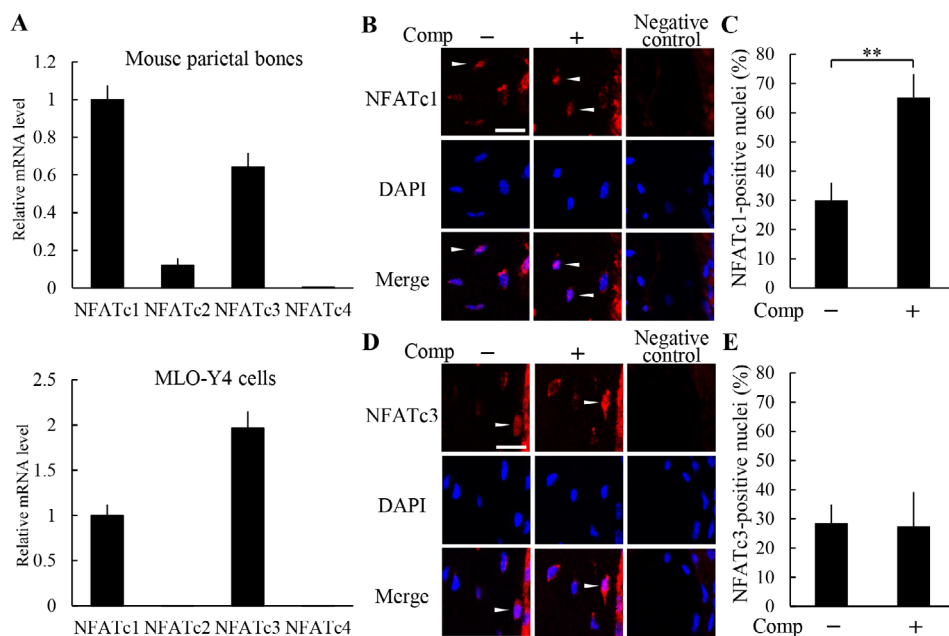


Fig 5 Compressive force induced nuclear translocation of NFATc1 in osteocytes. (A) NFATs mRNA expression level in mouse parietal bones and MLO-Y4 cells was analyzed by real-time PCR ($n = 3$). Nuclear translocation of NFATc1 (B,C) and NFATc3 (D,E) in the parietal bones of the nonloaded and loaded groups was analyzed by immunohistochemistry (B,D), and the ratio of positive nuclei in osteocytes (C,E) was calculated (four animals per group). Arrow-heads indicate the nuclear translocation of NFAT in osteocytes. Scale bar = $10 \mu\text{m}$. Comp = compressive force loading. $**P < 0.01$.

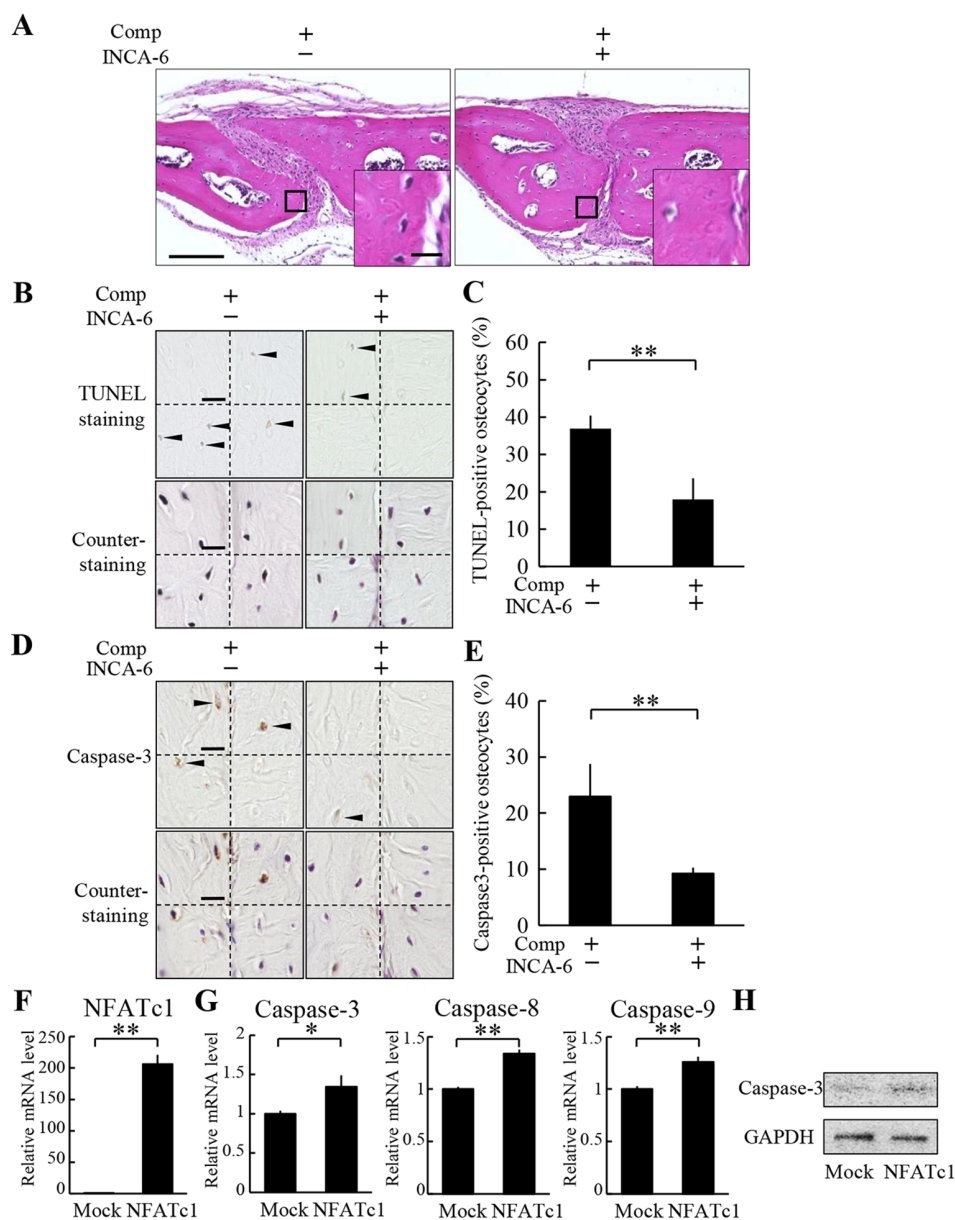


Fig 6 The induction of osteocyte apoptosis by compressive force loading is dependent on NFATc1. (A) Histological analysis of the parietal bones at 6 hours after application of compressive force was performed by H&E staining. INCA-6 was injected s.c. into the parietal bone area prior to the application of compressive force. A magnified picture of the ROI is shown in the lower right corner of each picture. Scale bar = 100 μ m, and 10 μ m in insets. (B) TUNEL staining and subsequent counterstaining with hematoxylin of the parietal bones were performed. All four ROIs in a section in each group are shown. Arrowheads indicate TUNEL-positive osteocytes. Comp = compressive force loading. Scale bar = 10 μ m. (C) TUNEL-positive ratio of osteocytes was calculated (four animals per group). $**P < 0.01$. (D) Caspase-3 immunohistochemistry and subsequent counterstaining with hematoxylin of the parietal bones were performed. All four ROIs in a section in each group are shown. Arrowheads indicate caspase-3-positive osteocytes. Scale bar = 10 μ m. (E) Caspase-3-positive ratio of osteocytes was calculated (four animals per group). $**P < 0.01$. (F-H) MLO-Y4 cells were infected with a lentiviral vector encoding NFATc1 or an empty vector (mock). The expression of mRNA of NFATc1 (F), and caspase-3, caspase-8, and caspase-9 (G) in MLO-Y4 cells were analyzed by real-time PCR. $*P < 0.05$, $**P < 0.01$; $n = 3$. (H) Cleaved caspase-3 expression was analyzed by Western blot.

significantly higher ratio than the nonloaded groups (Fig. 7A,B). In contrast, the ratio in the loaded group with MENK was $30.3 \pm 5.0\%$; it was significantly lower than the loaded group without MENK and was comparable to the nonloaded groups (Fig. 7A,B). The number of NFATc1-positive nuclei and the total number of nuclei were 3.0 ± 0 and 11.5 ± 1.9 , and 3.3 ± 0.5 and 10.8 ± 1.0 in the nonloaded groups without and with MENK, respectively,

and 6.8 ± 1.0 and 10.5 ± 2.7 , and 3.5 ± 1.0 and 11.5 ± 2.1 in the loaded groups without and with MENK, respectively. Ratios of NFATc3-positive nuclei in the nonloaded groups without and with MENK were $29.6 \pm 3.0\%$ and $29.6 \pm 3.0\%$, respectively (Fig. 7C,D). The ratios in the loaded groups without and with MENK were $26.0 \pm 8.8\%$ and $28.9 \pm 4.7\%$, respectively (Fig. 7C,D). There was no significant difference between any of the groups. The number

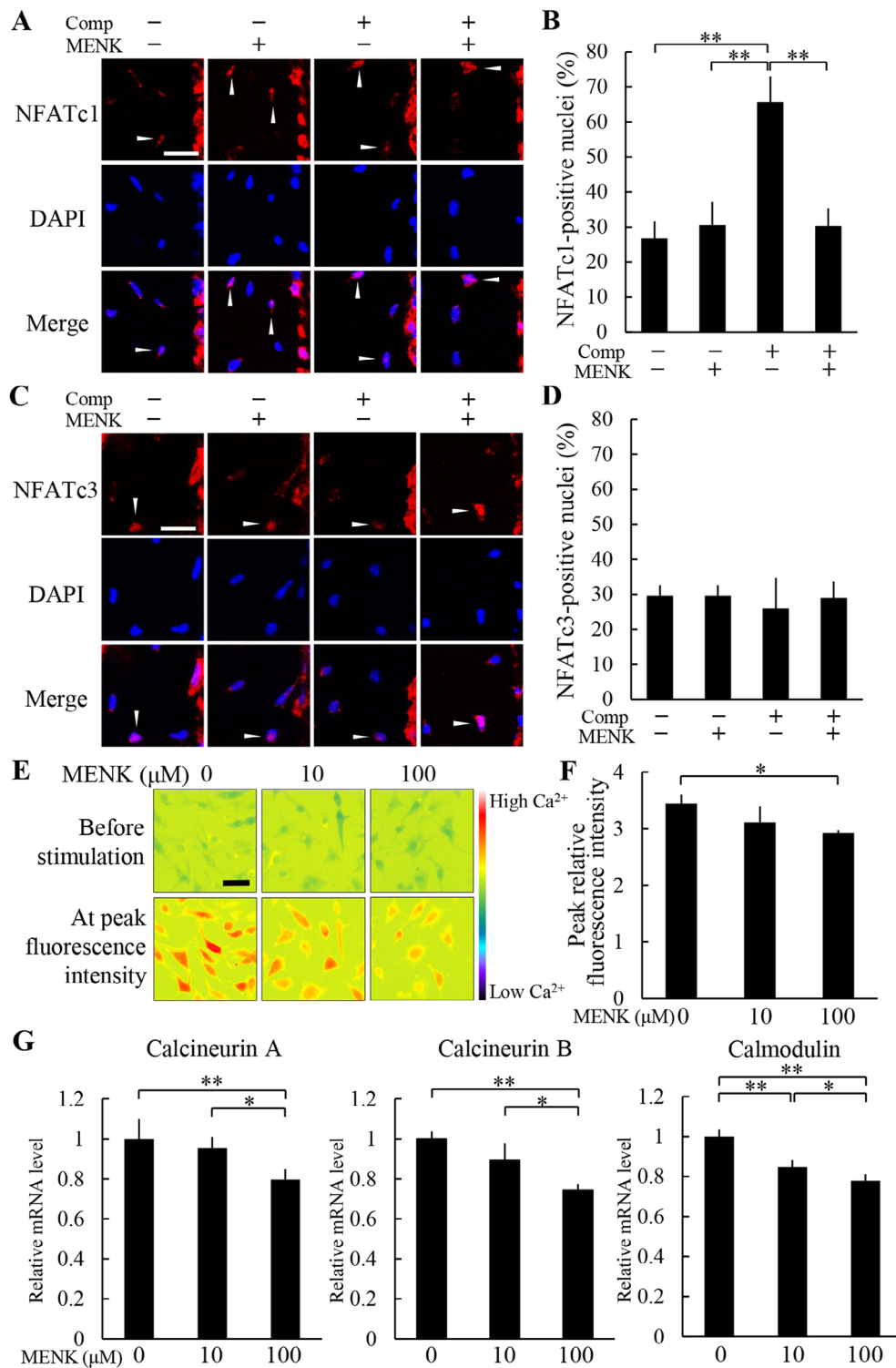


Fig 7 Methionine enkephalin (MENK) inhibited nuclear translocation of NFATc1 in the compressive force-loaded osteocytes. Nuclear translocation of NFATc1 (A,B) and NFATc3 (C,D) in the parietal bones at 6 hours after application of compressive force was analyzed by immunohistochemistry (A,C), and the ratio of positive nuclei in osteocytes (B,D) was calculated (four animals per group.). MENK was injected s.c. into the parietal bone area prior to the application of compressive force. Arrowheads indicate the nuclear translocation of NFAT in osteocytes. Scale bar = 10 μm . $**P < 0.01$. (E) Representative images of Fura-2 AM-loaded MLO-Y4 cells before ionomycin stimulation and at the time of peak fluorescence intensity after ionomycin stimulation. MLO-Y4 cells were treated with MENK for 24 hours before Ca^{2+} imaging. The color scale represents relative fluorescence intensity. Scale bar = 50 μm . (F) Fluorescence intensity before ionomycin treatment was regarded as 1 and the relative increase in Ca^{2+} was measured. Comp = compressive force loading. $*P < 0.05$; $n = 3$. (G) MLO-Y4 cells were treated with MENK for 24 hours, and the expression levels of calcineurin a, calcineurin B, and calmodulin mRNA in each group at day 2 culture were analyzed by real-time PCR. $*P < 0.05$, $**P < 0.01$; $n = 4$.

of NFATc3-positive nuclei and the total number of nuclei were 3.5 ± 0.6 and 11.8 ± 1.0 , 3.5 ± 0.6 , and 11.8 ± 1.0 in the non-loaded groups without and with MENK, respectively, 3.0 ± 1.4 and 11.3 ± 1.7 , and 3.0 ± 0.8 and 10.3 ± 1.3 in the loaded groups without and with MENK, respectively. These data indicated that MENK inhibited the nuclear translocation of NFATc1 in osteocytes induced by compressive force loading.

To further investigate the mechanisms by which MENK regulates nuclear translocation of NFATc1, we focused on Ca^{2+} signaling. Real-time Ca^{2+} imaging using the Ca^{2+} indicator dye Fura-2 AM showed that a Ca^{2+} ionophore ionomycin elevated the fluorescence intensity of intercellular Ca^{2+} in MLO-Y4 cells without MENK treatment (Fig. 7E,F). The elevation of fluorescence intensity by ionomycin was decreased by MENK treatment in a dose-dependent manner; higher concentration of MENK showed significant reduction of the relative increase in fluorescence compared with the MENK-nontreated control (Fig. 7E,F). Moreover, the expression of Ca^{2+} signaling mediators, calcineurin A, calcineurin B, and calmodulin in MLO-Y4 cells were assessed. Expression levels of these mRNAs were significantly decreased by MENK treatment in a dose-dependent manner (Fig. 7G).

Discussion

It is apparent that neuropeptides play important roles in bone metabolism, and the identification of neuropeptides that promote bone remodeling is a critical issue in bone biology.^(14–16) It is generally thought that neuropeptides are produced by nerve cells, but recent studies indicate that bone cells are also producers of neuropeptides. For instance, neuropeptide Y is produced by osteocytes and facilitates bone remodeling.⁽³⁷⁾ In the present study, we demonstrated, for the first time, that osteocytes produce an endogenous opioid MENK in the mouse parietal bones. In addition, we found the expression of DOR, a major receptor of MENK, in osteocytes. Osteocytes reside in lacunae within the mineralized bone matrix and have their dendritic processes through tiny tunnels called canaliculi, forming the osteocyte lacunocanalicular network via gap junctions.^(2,3,38,39) These findings suggest that MENK functions in an autocrine and/or paracrine manner in the osteocyte lacunocanalicular network.

Osteocytes are key players of mechanotransduction in bones; that is, they convert external mechanical stress into biochemical signaling.^(5,38) CTGF is known as a mechanoresponsive factor; its expression is upregulated by mechanical stress.^(12,13) It binds to candidate receptors, such as integrin, lipoprotein receptor-related protein-1, and tyrosine kinase receptor A; its signaling facilitates various biological processes, including proliferation, differentiation, and substrate production.^(40–43) We previously reported that increased expression of CTGF in osteocytes by compressive force induces osteocyte apoptosis *in vivo* and *in vitro*.^(12,13) In the present study, we loaded compressive force to the mouse parietal bones, resulting in a reduction of MENK expression in osteocytes. A neutralizing CTGF antibody inhibited the compressive force-induced reduction of MENK. Furthermore, we showed that an increase in osteocyte apoptosis in the compressive force-loaded parietal bones was inhibited by MENK administration. These results suggest that osteocyte apoptosis in response to compressive force is induced through suppression of MENK expression by CTGF signaling. Osteocyte apoptosis is regulated positively by glucocorticoids and oxidative stress-related factors and negatively regulated by PTH, estrogen, and androgen.⁽⁴⁴⁾ In addition to these factors, neuropeptides, including MENK, can be

considered novel regulators of osteocyte apoptosis according to the present study. Aging, loss of mechanical stress under a condition of weightlessness, and glucocorticoid-induced bone disease cause excessive osteocyte apoptosis and subsequent bone loss.^(45–47) Our finding about the inhibitory effect of MENK on osteocyte apoptosis may contribute to the development of treatments for abnormal bone loss caused by osteocyte apoptosis.

Because NFAT has a close relationship with apoptosis in various types of cells, we examined the role of NFAT in compressive force-induced osteocyte apoptosis. Our data showed that NFATc1 and NFATc3 mRNA were highly expressed in bone tissues and osteocytes. Nuclear translocation of NFATc1 in the osteocytes in the parietal bones was enhanced by compressive force, whereas that of NFATc3 was not. These results indicated that translocation of NFATc1, among NFATs, into nuclei was increased in response to the compressive force in osteocytes. INCA-6, which inhibits NFAT translocation into nuclei, suppressed the increase in osteocyte apoptosis in the compressive force-loaded parietal bones. Moreover, overexpression of NFATc1 induced expression of apoptosis-related genes and cleaved caspase-3 protein in MLO-Y4 cells. Our findings suggest that osteocyte apoptosis induced by compressive force is advanced through induction of NFATc1 nuclear translocation.

Furthermore, we analyzed the relationship between MENK and NFATc1 in the molecular regulation of osteocytes apoptosis. Our data showed that MENK administration reduced nuclear translocation of NFATc1 in osteocytes *in vivo*, suggesting that the decreased MENK expression promotes nuclear translocation of NFATc1 and following osteocyte apoptosis during osteocyte response to compressive force. It is known that the Ca^{2+} signaling pathway is a major mechanism of nuclear translocation of NFAT. That is, Ca^{2+} influx into cytoplasm leads to calmodulin-dependent activation of calcineurin, followed by NFAT dephosphorylation and nuclear translocation.⁽⁴⁸⁾ Importantly, the Ca^{2+} /calcineurin/NFAT pathway promotes apoptosis in various cells such as muscle cells, megakaryocytes, and mesangial cells.^(33,49,50) In the present study, we found that MENK suppressed Ca^{2+} influx and expression of calcineurin and calmodulin in osteocytes, indicating that MENK is a negative regulator of Ca^{2+} signaling. Taken together, MENK would negatively regulate osteocyte apoptosis through the suppression of the Ca^{2+} /calcineurin/NFATc1 pathway.

Ca^{2+} influx is an initial biochemical event of mechanical stress-loaded osteocytes; it stimulates osteocyte functions, such as gene expression and intercellular communication.⁽⁵¹⁾ Therefore, inhibition of Ca^{2+} influx by MENK may be an important mechanism to regulate mechanical stress-induced bone remodeling by regulating not only apoptosis, but other functions of osteocytes.

Conclusions

The present study revealed that osteocytes expressed MENK, whereas the MENK expression was suppressed by compressive force via CTGF signaling. Moreover, MENK inhibited compressive force-induced osteocyte apoptosis by downregulating nuclear translocation of NFATc1. MENK is considered to regulate nuclear translocation of NFATc1 by suppressing Ca^{2+} signaling in osteocytes. These results suggest that osteocyte-produced MENK is a competent neuropeptide that regulates bone remodeling driven by mechanical stress. Our findings about novel roles of MENK in osteocytes not only contribute to understanding the mechanisms of bone remodeling regulated by neuropeptides, but are also possibly applicable to the development of treatments for pathological bone loss.

Disclosures

All authors state that they have no conflicts of interest.

Acknowledgments

This study was supported by a Grant-in-Aid for scientific Research (15H05048 to TT-Y and 18 K09828 to NT) from the Japan Society for the Promotion of Science. We thank the Biomedical Research Unit of Tohoku University Hospital for their technical equipment support.

Authors' roles: Study design: TT-Y, CS, and NT. Study conduct: TT-Y, CS, and NT. Data collection: CS, NT, JW, KS, TM, MY, TO, AI, SK, DS, IT, and YS. Data analysis: CS and NT. Data interpretation: TT-Y, CS, and NT. Drafting manuscript: TT-Y, CS, and NT. Revising manuscript content: All. Approving final version of manuscript: All. TT-Y takes responsibility for the integrity of the data analysis.

References

- Huiskes R, Ruimerman R, van Lenthe GH, Janssen JD. Effects of mechanical forces on maintenance and adaptation of form in trabecular bone. *Nature*. 2000;405:704–6.
- Tanaka-Kamioka K, Kamioka H, Ris H, Lim SS. Osteocyte shape is dependent on Actin filaments and osteocyte processes are unique Actin-rich projections. *J Bone Miner Res*. 1998;13(10):1555–68.
- Dallas SL, Prideaux M, Bonewald LF. The osteocyte: an endocrine cell ... and more. *Endocr Rev*. 2013;34(5):658–90.
- Tatsumi S, Ishii K, Amizuka N, et al. Targeted ablation of osteocytes induces osteoporosis with defective mechanotransduction. *Cell Metab*. 2007;5(6):464–75.
- Takano-Yamamoto T. Osteocyte function under compressive mechanical force. *Jpn Dent Sci Rev*. 2014;50:29–39.
- Nakashima T, Hayashi M, Takayanagi H. New insights into osteoclastogenic signaling mechanisms. *Trends Endocrinol Metab*. 2012;23(11):582–90.
- Takano-Yamamoto T, Sasaki K, Fatemeh G, et al. Synergistic acceleration of experimental tooth movement by supplementary high-frequency vibration applied with a static force in rats. *Sci Rep*. 2017;7(1):13969.
- Sakamoto M, Fukunaga T, Sasaki K, et al. Vibration enhances osteoclastogenesis by inducing RANKL expression via NF- κ B signaling in osteocytes. *Bone*. 2019;123:56–66.
- Noble BS, Peet N, Stevens HY, et al. Mechanical loading: biphasic osteocyte survival and targeting of osteoclasts for bone destruction in rat cortical bone. *Am J Physiol Cell Physiol*. 2003;284(4):C934–43.
- Kogianni G, Mann V, Noble BS. Apoptotic bodies convey activity capable of initiating osteoclastogenesis and localized bone destruction. *J Bone Miner Res*. 2008;23(6):915–27.
- Cardoso L, Herman BC, Verborgt O, Laudier D, Majeska RJ, Schaffler MB. Osteocyte apoptosis controls activation of intracortical resorption in response to bone fatigue. *J Bone Miner Res*. 2009;24(4):597–605.
- Sakai Y, Balam TA, Kuroda S, et al. CTGF and apoptosis in mouse osteocytes induced by tooth movement. *J Dent Res*. 2009;88(4):345–50.
- Hoshi K, Kawaki H, Takahashi I, et al. Compressive force-produced CCN2 induces osteocyte apoptosis through ERK1/2 pathway. *J Bone Miner Res*. 2014;29(5):1244–57.
- Ducy P, Amling M, Takeda S, et al. Leptin inhibits bone formation through a hypothalamic relay: a central control of bone mass. *Cell*. 2000;100(2):197–207.
- Baldock PA, Sainsbury A, Couzens M, et al. Hypothalamic Y2 receptors regulate bone formation. *J Clin Invest*. 2002;109(7):915–21.
- Lee NJ, Nguyen AD, Enriquez RF, et al. Osteoblast specific Y1 receptor deletion enhances bone mass. *Bone*. 2011;48(3):461–7.
- Mansour A, Hoversten MT, Taylor LP, Watson SJ, Akil H. The cloned mu, delta and kappa receptors and their endogenous ligands: evidence for two opioid peptide recognition cores. *Brain Res*. 1995;700(1–2):89–98.
- Goto S, Morigaki R, Okita S, Nagahiro S, Kaji R. Development of a highly sensitive immunohistochemical method to detect neurochemical molecules in formalin-fixed and paraffin-embedded tissues from autopsied human brains. *Front Neuroanat*. 2015;9:22.
- Lu Y, McNearney TA, Lin W, Wilson SP, Yeomans DC, Westlund KN. Treatment of inflamed pancreas with enkephalin encoding HSV-1 recombinant vector reduces inflammatory damage and behavioral sequelae. *Mol Ther*. 2007;15(10):1812–9.
- Bhargava HN, Matwyshyn GA, Hanissian S, Tejwani GA. Opioid peptides in pituitary gland, brain regions and peripheral tissues of spontaneously hypertensive and Wistar-Kyoto normotensive rats. *Brain Res*. 1988;440(2):333–40.
- Elhassan AM, Lindgren JU, Hultenby K, Bergstrom J, Adem A. Methionine-enkephalin in bone and joint tissues. *J Bone Miner Res*. 1998;13(1):88–95.
- Queiroz-Junior CM, Maltos KL, Pacheco DF, Silva TA, Albergaria JD, Pacheco CM. Endogenous opioids regulate alveolar bone loss in a periodontal disease model. *Life Sci*. 2013;93(12–14):471–7.
- Zagon IS, Wu Y, McLaughlin PJ. Opioid growth factor and organ development in rat and human embryos. *Brain Res*. 1999;839(2):313–22.
- King T, Vardanyan A, Majuta L, et al. Morphine treatment accelerates sarcoma-induced bone pain, bone loss, and spontaneous fracture in a murine model of bone cancer. *Pain*. 2007;132(1–2):154–68.
- Rosen H, Krichevsky A, Bar-Shavit Z. The enkephalinergic osteoblast. *J Bone Miner Res*. 1998;13(10):1515–20.
- Rosen H, Polakiewicz RD, Benzakine S, Bar-Shavit Z. Proenkephalin A in bone-derived cells. *Proc Natl Acad Sci USA*. 1991;88(9):3705–9.
- McTavish N, Copeland LA, Saville MK, Perkins ND, Spruce BA. Proenkephalin assists stress-activated apoptosis through transcriptional repression of NF- κ B- and p53-regulated gene targets. *Cell Death Differ*. 2007;14(9):1700–10.
- Tang B, Zhang Y, Liang R, et al. Activation of the δ -opioid receptor inhibits serum deprivation-induced apoptosis of human liver cells via the activation of PKC and the mitochondrial pathway. *Int J Mol Med*. 2011;28(6):1077–85.
- Narita M, Kuzumaki N, Miyatake M, et al. Role of delta-opioid receptor function in neurogenesis and neuroprotection. *J Neurochem*. 2006;97(5):1494–505.
- Takano-Yamamoto T, Fukunaga T, Takeshita N. Gene expression analysis of CCN protein in bone under mechanical stress. *Methods Mol Biol*. 2017;1489:283–308.
- Li Y, Ren W, Wang X, et al. MicroRNA-150 relieves vascular remodeling and fibrosis in hypoxia-induced pulmonary hypertension. *Biomed Pharmacother*. 2019;109:1740–9.
- Tan Z, Kang T, Zhang X, Tong Y, Chen S. Nerve growth factor prevents arsenic-induced toxicity in PC12 cells through the AKT/GSK-3 β /NFAT pathway. *J Cell Physiol*. 2019;234(4):4726–38.
- Soni H, Adebijoyi A. TRPC6 channel activation promotes neonatal glomerular mesangial cell apoptosis via calcineurin/NFAT and FasL/Fas signaling pathways. *Sci Rep*. 2016;6:29041.
- Lu WC, Xie H, Tie XX, Wang R, Wu AH, Shan FP. NFAT-1 hyperactivation by methionine enkephalin (MENK) significantly induces cell apoptosis of rats C6 glioma in vivo and in vitro. *Int Immunopharmacol*. 2018;56:1–8.
- Sugawara Y, Ando R, Kamioka H, et al. The alteration of a mechanical property of bone cells during the process of changing from osteoblasts to osteocytes. *Bone*. 2008;43(1):19–24.
- Takeshita N, Hasegawa M, Sasaki K, et al. In vivo expression and regulation of genes associated with vascularization during early response of sutures to tensile force. *J Bone Miner Metab*. 2017;35(1):40–51.
- Igwe JC, Jiang X, Paic F, et al. Neuropeptide Y is expressed by osteocytes and can inhibit osteoblastic activity. *J Cell Biochem*. 2009;108(3):621–30.

38. Klein-Nulend J, Bakker AD, Bacabac RG, Vatsa A, Weinbaum S. Mechanosensation and transduction in osteocytes. *Bone*. 2013;54(2):182–90.
39. Kamioka H, Ishihara Y, Ris H, et al. Primary cultures of chick osteocytes retain functional gap junctions between osteocytes and between osteocytes and osteoblasts. *Microsc Microanal*. 2007;13(2):108–17.
40. Nishida T, Nakanishi T, Asano M, Shimo T, Takigawa M. Effects of CTGF/Hcs24, a hypertrophic chondrocyte-specific gene product, on the proliferation and differentiation of osteoblastic cells in vitro. *J Cell Physiol*. 2000;184(2):197–206.
41. Shimo T, Nakanishi T, Nishida T, et al. Connective tissue growth factor induces the proliferation, migration, and tube formation of vascular endothelial cells in vitro, and angiogenesis in vivo. *J Biochem*. 1999;126(1):137–45.
42. Nishida T, Kawaki H, Baxter RM, Deyoung RA, Takigawa M, Lyons KM. CCN2 (connective tissue growth factor) is essential for extracellular matrix production and integrin signaling in chondrocytes. *J Cell Commun Signal*. 2007;1(1):45–58.
43. Kawaki H, Kubota S, Suzuki A, et al. Cooperative regulation of chondrocyte differentiation by CCN2 and CCN3 shown by a comprehensive analysis of the CCN family proteins in cartilage. *J Bone Miner Res*. 2008;23(11):1751–64.
44. Plotkin LI. Apoptotic osteocytes and the control of targeted bone resorption. *Curr Osteoporos Rep*. 2014;12(1):21–6.
45. Almeida M, Han L, Martin-Millan M, et al. Skeletal involution by age-associated oxidative stress and its acceleration by loss of sex steroids. *J Biol Chem*. 2007;282(37):27285–97.
46. Weinstein RS, Jilka RL, Parfitt AM, Manolagas SC. Inhibition of osteoblastogenesis and promotion of apoptosis of osteoblasts and osteocytes by glucocorticoids. Potential mechanisms of their deleterious effects on bone. *J Clin Invest*. 1998;102(2):274–82.
47. Aguirre JI, Plotkin LI, Stewart SA, et al. Osteocyte apoptosis is induced by weightlessness in mice and precedes osteoclast recruitment and bone loss. *J Bone Miner Res*. 2006;21(4):605–15.
48. Mognol GP, Carneiro FR, Robbs BK, Faget DV, Viola JP. Cell cycle and apoptosis regulation by NFAT transcription factors: new roles for an old player. *Cell Death Dis*. 2016;7:e2199.
49. Benavides Damm T, Egli M. Calcium's role in mechanotransduction during muscle development. *Cell Physiol Biochem*. 2014;33(2):249–72.
50. Arabanian LS, Kujawski S, Habermann I, Ehninger G, Kiani A. Regulation of fas/fas ligand-mediated apoptosis by nuclear factor of activated T cells in megakaryocytes. *Br J Haematol*. 2012;156(4):523–34.
51. Miyauchi A, Notoya K, Mikuni-Takagaki Y, et al. Parathyroid hormone-activated volume-sensitive calcium influx pathways in mechanically loaded osteocytes. *J Biol Chem*. 2000;275(5):3335–42.